NANO LETTERS

Letter

pubs.acs.org/NanoLett

Large-Scale Synthesis of High-Quality Hexagonal Boron Nitride Nanosheets for Large-Area Graphene Electronics

Kang Hyuck Lee,[†,∥] Hyeon-Jin Shin,[‡,∥] Jinyeong Lee,[†] In-yeal Lee,[§] Gil-Ho Kim,[§] Jae-Young Choi,*[,‡] and Sang-Woo Kim*[,†]

[†]School of Advanced Materials Science and Engineering, SKKU Advanced Institute of Nanotechnology (SAINT), Center for Human Interface Nanotechnology (HINT), SKKU-Samsung Graphene Center, Sungkyunkwan University (SKKU), Suwon 440-746, Republic of Korea

[‡]Graphene Center, Samsung Advanced Institute of Technology, Yongin 446-712, Republic of Korea

[§]SKKU Advanced Institute of Nanotechnology (SAINT), Department of Electronic and Electrical Engineering, Sungkyunkwan University (SKKU), Suwon 440-746, Republic of Korea

S *Supporting Information*

ABSTRACT: Hexagonal boron nitride (h-BN) has received a great deal of attention as a substrate material for high-performance graphene electronics because it has an atomically smooth surface, lattice constant similar to that of graphene, large optical phonon modes, and a large electrical band gap. Herein, we report the large-scale synthesis of high-quality h-BN nanosheets in a chemical vapor deposition (CVD) process by controlling the surface morphologies of the copper (Cu) catalysts. It was found that morphology control of the Cu foil is much critical for the formation of the pure h-BN nanosheets as well as the improvement of their crystallinity. For the first time, we demonstrate the performance enhancement of CVD-based graphene devices with large-scale h-BN nanosheets. The mobility of the graphene device on the h-BN nanosheets was increased 3 times compared to that without the h-BN nanosheets. The on−off ratio of the drain current is 2 times higher than that of the graphene device without h-BN. This work suggests that high-quality h-BN nanosheets based on CVD are very promising for high-performance large-area graphene electronics.

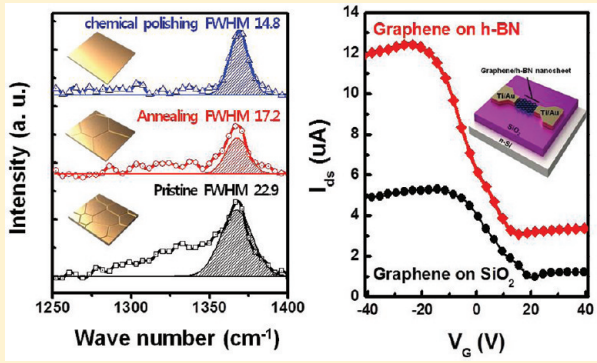

KEYWORDS: *Hexagonal boron nitride nanosheets, chemical vapor deposition, morphology control, large-scale synthesis, chemical polishing, graphene device*

Hexagonal boron nitride (h-BN) is a layered material with a graphite-type structure in which planar networks of BN hexagons are regularly stacked. h-BN with a wide band gap (~5.9 eV)[1] has many attractive properties for potential applications, for instance, high temperature stability, high mechanical strength, a large thermal conductivity, and a low dielectric constant.[2−6] Recently, h-BN has received a great deal of attention as a promising material substrate for high-quality graphene electronics because it has an atomically smooth surface that is relatively free of dangling bonds and charge traps. It also has a similar lattice constant to graphene[7] and should enable the tuning of its band gap.[8] However, h-BN monolayers are generally produced by the micromechanical cleavage of a bulk h-BN crystal, which is limited to small sizes and suitable techniques.[9,10] For practical applications, the realization of high-quality and large-area h-BN consisting a homogeneous monolayer or a few layers is essential.

Recently, reproducible and scalable chemical vapor deposition (CVD) processes for fabricating few-layer h-BN films on transition metal surfaces have been reported.[11,12] Although large-area few-layer h-BN films have been successfully realized using the CVD process, there are still many issues which remain to be resolved, including the formation of defects such as allotropes (amorphous BN (a-BN) and cubic BN (c-BN)) and the generation of impurity particles with a heterostructure ($B_xC_yN_z$/BN soot) on the h-BN surface. Thus, the achievement of large-scale high-quality h-BN layers with a low density of defects and impurity particles is strongly desirable to facilitate more fundamental studies and industrial applications with two-dimensional layered nanomaterials.

Herein, we demonstrate a facile method of growing large-scale high-quality h-BN nanosheets by controlling the surface morphology of copper (Cu) foils acting as a catalyst. The thermal annealing and chemical polishing of the Cu foil lead to an increase in its grain size and surface flatness. It was found that increasing the grain size and improving the flatness of the

Received: October 15, 2011
Revised: December 15, 2011
Published: January 5, 2012

   dx.doi.org/10.1021/nl203635v | *Nano Lett.* 2012, 12, 714−718

surface of Cu result in the reduction in the amount of allotropes (c-BN) and impurity particles that are crucial for high-quality h-BN growth. Furthermore, we characterize for the first time the electrical properties of large-scale CVD-grown graphene on CVD-grown h-BN nanosheets. A field effect transistor (FET) based on graphene was fabricated utilizing the large-scale h-BN nanosheets as a buffer layer on a SiO_2 gate dielectric. The mobility and on/off ratio of the drain current (I_{ds}) of the CVD-grown graphene FET with h-BN nanosheets grown on the thermally annealed and chemically polished Cu foil were improved by 3 and 2 times as compared to that of the CVD-grown graphene FET without the h-BN nanosheets, respectively. This implies that large-scale high-quality h-BN nanosheets should be useful for high-performance large-area graphene electronics.

The synthesis of h-BN layers was carried out in an ambient pressure CVD system as described in a previous work.[11] For the growth process, a Cu foil (Alpha Acer, 125 μm thickness) was placed in the CVD chamber and gradually heated up to 1000 °C for 2 h 30 min in a mixed Ar/H_2 (20 vol % H_2, 80 vol % Ar) flow with a flow rate of 100 sccm. Then, the main growth was carried out in a mixed Ar/H_2 gas flow of 75 sccm for 30 min at 1000 °C with ammonia borane (NH_3–BH_3) as the source material sublimated at 110–130 °C using a subheating chamber with an N_2 gas flow of 25 sccm. It is known that such a sublimation temperature leads to the formation of a hydroborazine structure by cyclization.[13] Finally, after the main growth, the chamber was cooled to 180 °C with a mixed Ar/H_2 gas flow at a flow rate of 100 sccm for 4 h. After the synthesis, the nanosheets were coated with poly(methyl methacrylate) (PMMA) and immersed in Cu etchant (Transene, type 1) in order to etch away the Cu foil. When the Cu was completely etched away, the h-BN nanosheets with PMMA were rinsed in deionized water several times to wash away the etchant residues. Then, the PMMA-coated h-BN nanosheets were transferred onto a SiO_2 substrate for further characterization and device fabrication.[14,15]

The optical image of the h-BN film transferred onto the SiO_2/Si substrate is shown in Figure 1a. Although this film is quite uniform and continuous, some particles (red arrow) were observed. The surface roughness measured by atomic force microscopy (AFM, Dimension V, Veeco Co.) in tapping mode provides further insight into the degree of uniformity. The surface of the h-BN film was fairly flat over an area over 200 × 200 nm^2. The root-mean-square (rms) roughness of this film was 0.45 nm, which is lower than that of SiO_2, viz. 0.64 nm (see Supporting Information Figure S1a,b). However, the surface of h-BN inspected over an area of 1 × 1 μm^2 was rough with an rms roughness of 2.42 nm (see Supporting Information Figure S1c), showing a similar signal to that observed in the optical image (Figure 1a). The BN structures were characterized by Raman spectroscopy (Renishaw, RM-1000 Invia, 514 nm, Ar^+ ion laser) which provides spectral bands that can be extracted by deconvoluting them into three components: B–N vibration mode (E_{2g}) within h-BN (1367 cm^{-1}),[16] boron carbon nitride ($B_xC_yN_z$) and/or BN soot (between 1322 and 1350 cm^{-1}), which was not clearly identified,[17,18] and T2 symmetry of c-BN (1304 cm^{-1}), in order to obtain more abundant information.[19] Even though the films were dominantly composed of the h-BN layer, the formation of BN allotropes could not be ruled out. Furthermore, the effect of the BN allotropes on the graphene device was not clearly understood. To confirm the reliability of the h-BN nanosheets for device applications, a graphene FET

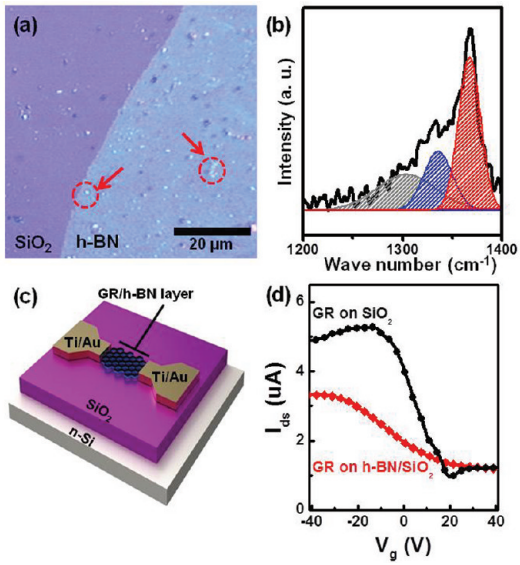

Figure 1. (a) Optical image of h-BN nanosheets transferred onto the SiO_2/Si substrate. The red arrows indicate particles. (b) Raman spectrum of h-BN nanosheets exited by 514 nm laser which is decomposed into c-BN (shaded area in gray), $B_xC_yN_z$ or/and BN soot (shaded area in blue), and h-BN (shaded area in red). (c) Schematic of graphene (GR) device structure with growth h-BN nanosheets. (d) Measured I_{ds}–V_g curves of the monolayer graphene FETs without/with h-BN nanosheets under ambient conditions.

was fabricated in a similar manner to that in a previous report based on the mechanical cleavage of graphene and h-BN, as shown in Figure 1c.[10] The CVD-grown h-BN nanosheets and CVD-grown monolayer graphene were transferred onto a SiO_2/heavily doped Si (n^{++} Si) substrate in sequence (see Supporting Information Figure S2). The subsequent formation of source and drain electrodes with Ti/Au (5 nm/200 nm) was realized by a photolithography technique. The channel length and width were 10 μm and 2 μm, respectively.

The transfer characteristics (I_{ds}–V_g) curve of the monolayer graphene FET without h-BN nanosheets measured under ambient conditions shows p-type behavior and the upshift of the Dirac point at V_g = 20 V (black line in Figure 1d). Unfortunately, the electron transfer of the graphene FET on the h-BN nanosheets indicated not only the upshift of the Dirac point to over V_g = 40 V but also the decrease of the on-current of the drain, which were different from the results obtained in a previous work (red line in Figure 1d).[10] These results indicate that the quality of the grown h-BN is not sufficient for it to be applied to devices due to the presence of impurity particles and heterostructures mixed with the c-BN, as shown in Figure 1a,b. The improvement in the flatness and crystallinity of h-BN is one of the most important goals to realize high-performance graphene electronics using h-BN nanosheets.

In general, B atoms are highly soluble in diverse transition metals at high temperature near 1000 °C, whereas N atoms are nearly insoluble.[20,21] Therefore, it can be suggested that the h-BN nanosheets were grown by the recrystallization of the polymeric BN-ring by the adsorption of the cyclic-BN structure on the metal surface.[12] The quality of a thin film grown on a metal by surface adsorption is strongly affected by the surface morphology, as previously reported in the case of the graphene growth mechanism on a Cu foil.[22,23] In this regard, we introduced two methods (thermal annealing (TA) and thermal

dx.doi.org/10.1021/nl203635v | Nano Lett. 2012, 12, 714–718

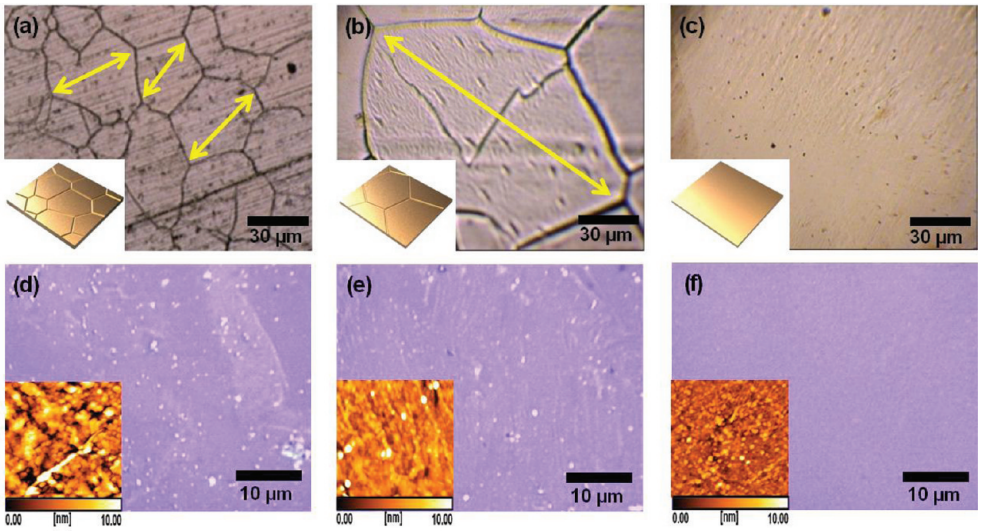

Figure 2. Optical images of Cu foils prepared by (a) pristine, (b) TA at 1020 °C for 2 h, and (c) TA (1020 °C for 2 h)/CP. The inset images in (a–c) reveal the schematic illustrations of the morphology-controlled Cu foils. Optical images showing surface morphologies of h-BN nanosheets transferred onto SiO_2/Si substrates after the growth of the h-BN nanosheets on (d) pristine Cu foil, (e) TA-treated Cu foil, and (f) TA/CP-treated Cu foil. The inset images of (d–f) show the corresponding AFM images (scan area is 1 × 1 μm^2).

annealing/chemical polishing (TA/CP)) to control the surface morphology of the Cu foil. The untreated (pristine) Cu foil with small grains having a size of ~30 um was changed to flat Cu foil with large grains having a size of ~120 um size after thermal annealing at 1020 °C for 2 h in an Ar atmosphere, as shown in Figure 2a,b. The flat surface morphology of the TA/CP-treated Cu foil was made by rubbing with Cu etchant (Transene, type1) after thermal annealing, as shown in Figure 2c. The surface roughness was measured by AFM which was gradually smooth after treatment (see Supporting Information Figure S3). The insets of Figure 2a–c show the schematic illustrations of the morphology-controlled Cu foils.

The h-BN nanosheets grown on the Cu foils were transferred onto SiO_2 (300 nm thick)/Si wafer as shown in Figure 2d–f. The number of impurity particles in the h-BN nanosheets grown on the TA-treated Cu foil is slightly decreased as compared to that in the h-BN nanosheets grown on the pristine Cu foil (Figure 2d,e). Moreover, the formation of impurity nanoparticles in the h-BN nanosheets grown on the TA/CP-treated Cu foil is dramatically suppressed (Figure 2f), resulting in large-area nanosheets with an atomically flat surface roughness. The AFM images over an area of 1 × 1 μm^2 provide further insight into the surface roughness of the treated Cu foils (insets of Figure 2d–f). The h-BN nanosheets grown on the pristine Cu foil have a rough surface morphology with an rms roughness of 2.42 nm. The h-BN nanosheets grown on the TA-treated Cu foil are slightly smoother with an rms roughness of less than 1.57 nm. On the other hand, the surface rms roughness of the h-BN nanosheets grown on the TA/CP-treated Cu foil is 1.10 nm. These results suggest that the flat surface and large grain size of the catalyst layer are essential to suppress the formation of impurity nanoparticles in the h-BN nanosheets.

To elucidate the dependence of the morphology on the treatment of the Cu foil more clearly, the structural quality of the h-BN nanosheets grown on the morphology-controlled Cu foils was further investigated using Raman spectroscopy (Figure 3a). The TA-treated Cu foil facilitated the formation of the h-BN phase by suppressing the formation of c-BN and boron

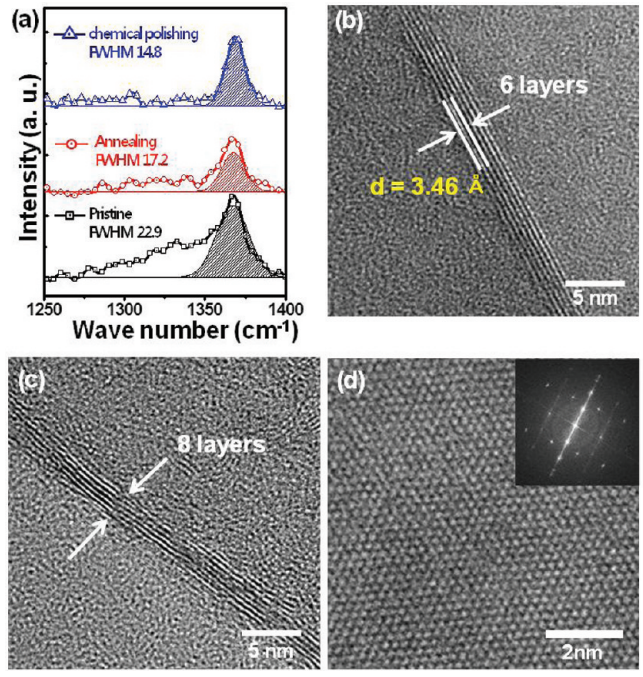

Figure 3. (a) Raman spectra of h-BN nanosheets grown on individual Cu foils at 514 nm. The shade was extracted by deconvoluting the h-BN peak. (b, c) Cross-sectional TEM images of h-BN nanosheets grown on the TA/CP-treated Cu foil. (d) HR TEM image showing hexagonal atomic arrays as well as its corresponding FFT pattern.

carbon nitride ($B_xC_yN_z$) and/or BN soot, as confirmed by the peaks near 1304 cm^{-1} and near 1336 cm^{-1}, respectively. Eventually, the TA/CP treatment of the Cu foil caused the allotropes to disappear from the modulated Cu surface. The origins of particles were more clearly characterized by confocal Raman mapping (see Supporting Information Figure S4). Effective surface diffusion of the adsorbed BN rings for the formation of atomically flat BN surface is restricted on a Cu foil with a rough surface morphology. The rough surface usually contains a large number of defects such as excess vacancies,

dx.doi.org/10.1021/nl203635v | Nano Lett. 2012, 12, 714–718

dislocations, and grain boundaries that are suitable heterogeneous nucleation sites. Thus, the formation of the impurity particles is proposed by three-dimensional Volmer–Weber nucleation along the rough surface area on the Cu foil.

In addition, the full width at half-maximum (fwhm) value of the h-BN peak near 1367 cm^{-1} was changed lower to 14.8 cm^{-1} compared with that of the h-BN grown on the pristine Cu foil about 22.9 cm^{-1}. This sharpness of the fwhm in the Raman spectrum can be ascribed to the increase in the individual grain size of the h-BN,[24] which may constitute evidence of strong dependency on the surface morphology of the Cu foil. Therefore, it was found that morphology control of the Cu foil is much critical for the formation of the pure h-BN nanosheets as well as the improvement of their crystallinity. The structural properties of the h-BN nanosheets grown on the TA/CP-treated Cu foil were additionally investigated by transmission electron microscopy (TEM, JEM 2100F, JEOL). It was found in the cross-sectional TEM results that the h-BN nanosheets have 6–8 atomic layers, as shown in Figure 3b,c. The observed interlayer distance of the h-BN nanosheets is nearly 3.46 Å, which is similar to that of bulk h-BN. Figure 3d shows the high-resolution (HR) TEM image showing hexagonal atomic arrays as well as its corresponding fast Fourier transfer (FFT) pattern, indicating the single-crystalline nature of the examined area.

Figure 4a shows the I_{ds}–V_g characteristics of FETs fabricated using two-type graphene structures: one with the h-BN nanosheets obtained from the TA/CP-treated Cu foil and the other without the h-BN nanosheets. The device structure is the same as that shown in Figure 1c. Each device has a L of 10 μm and W of 2 μm. The transfer curves measured under ambient conditions show p-type behavior. The Dirac point of the graphene device with the high-quality h-BN nanosheets is downshifted to V_g = 13 V as compared to that of the graphene device without h-BN, which is observed at V_g = 20 V. In addition, the on–off ratio of the I_{ds} of the graphene device with the h-BN nanosheets is 2 times higher than that of the graphene device without the h-BN nanosheets. The hole mobility was calculated from the linear regime of the transfer characteristics using the equation

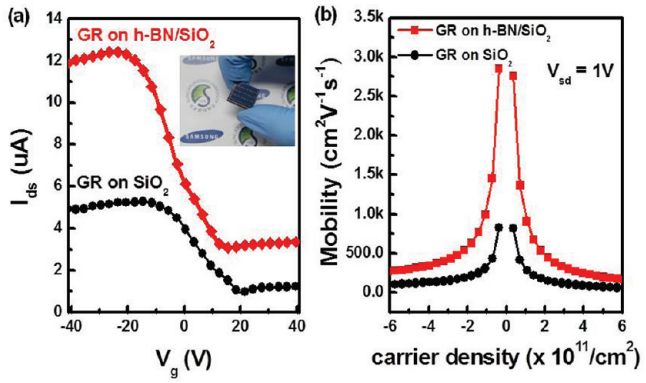

Figure 4. (a) I_{ds}–V_g characteristics of graphene (GR) TFTs on bare SiO_2 and high-quality h-BN nanosheets in atmospheric ambient. The inset is an optical image of the TFT arrays. (b) Mobility as a function of charge carrier density in graphene.

$$\mu_{FE} = \frac{1}{C_g}\frac{d\sigma}{dV_g} = \frac{L}{C_g W V_d}\frac{dI_d}{dV_g} = g_m \frac{L}{V_d W C_g}$$

where C_g is the measured gate capacitance of the dielectrics, I_{sd} is the drain current, V_g is the gate voltage, and μ_{FE} is the field-effect mobility. dI_d/dV_g was calculated from the slope between V_g = −50 and V_{Dirac} (V_g at Dirac point). The calculated hole carrier mobility (μ_h) of graphene on SiO_2 was 2560 $cm^2\ V^{-1}\ s^{-1}$ at V_{ds} = 1 V, whereas the μ_h of graphene assisted by the h-BN nanosheets was 6850 $cm^2\ V^{-1}\ s^{-1}$ at V_{ds} = 1 V. The carrier density (n) and mobilities (μ) can be extracted by applying a plane capacitor model (Drude model, $\mu = (ne\rho)^{-1}$ (e = electric charge, ρ = resistivity)), as shown in Figure 4b. The tunable carrier density (n_s) corresponds to the estimated charge induced by V_g, $n_s = C_g(V_g - V_{Dirac})/e$ ($V_{Dirac} = V_g$ at Dirac point), assuming a gate capacitance (C_g) of 115 aF μm^{-2} obtained from the geometrical considerations.[25] Even though the absolute value of the mobility is low due to the contact resistance in the two probe system, the μ_h of graphene assisted by the h-BN nanosheets is 3-fold higher (~573 $cm^2\ V^{-1}\ s^{-1}$ at $-2 \times 10^{11}/cm^2$) than that of graphene on SiO_2 (~199 $cm^2\ V^{-1}\ s^{-1}$ at $-2 \times 10^{11}/cm^2$). In comparison with the mobility calculated from the linear regime of the transfer characteristics, a similar improvement was observed.

In conclusion, we studied the influence of the Cu morphology on the high-quality growth of h-BN nanosheets. The number of impurity particles on the h-BN nanosheets and roughness of the Cu foil were strongly dependent on whether the Cu substrate was subjected to thermal annealing and chemical polishing or not. Furthermore, the flatness with large grain boundary and low rms were affect to decrease heterostructure (c-BN/BN soot). It was found that the key roles of the morphology control of the Cu catalyst are not only the formation of pure h-BN nanosheets with an atomically flat surface but also the improvement of the crystallinity. For the first time, the performance of large-area graphene devices based on high-quality h-BN nanosheets grown using the CVD approach was investigated, and a 3-fold higher mobility and on/off ratio were achieved. We expect that our approach can provide a beneficial method of preparing high-quality h-BN nanosheets to be utilized in high-performance large-area graphene electronics in the future.

■ ASSOCIATED CONTENT

Supporting Information

Surface morphology of SiO_2 and h-BN nanosheets grown on the pristine Cu foil (Figure S1), schematic illustration of the fabrication of graphene FETs based on h-BN (Figure S2), surface morphology of Cu foil according to treatment (Figure S3), and confocal Raman mapping of the h-BN nanosheet grown on the pristine Cu foil (Figure S4). This material is available free of charge via the Internet at http://pubs.acs.org.

■ AUTHOR INFORMATION

Corresponding Author

*E-mail: kimsw1@skku.edu (S.W.K.), jaeyoung88.choi@samsung.com (J.Y.C.).

Author Contributions

[||]These authors contributed equally to this work.

■ ACKNOWLEDGMENTS

This work was financially supported by the International Research & Development Program of the National Research Foundation of Korea (NRF) funded by the Ministry of Education, Science and Technology (MEST) (2010-00297),

Basic Science Research Program through the NRF funded by the MEST (2010-0015035), the Global Frontier Research Center for Advanced Soft Electronics through the NRF funded by the MEST, and the promotion program for the core faculty of Sungkyunkwan University (2011).

REFERENCES

(1) Watanabe, K.; Taniguchi, T.; Kanda, H. *Nature Mater.* **2004**, *3*, 404−409.
(2) Kho, J.-G.; Moon, K.-T.; Kim, J.-H.; Kim, D.-P. *J. Am. Ceram. Soc.* **2000**, *83* (11), 2681−2683.
(3) Sugino, T.; Tai, T. *Jpn. J. Appl. Phys., Part 2* **2000**, *39* (11A), L1101−L1104.
(4) Haubner, R.; Wilhelm, M.; Weissenbacher, R.; Lux, B. *Struct. Bonding (Berlin)* **2002**, *102*, 1−45.
(5) Kubota, Y.; Watanabe, K.; Tsuda, O.; Taniguchi, T. *Science* **2007**, *317* (5840), 932−934.
(6) Watanabe, K.; Taniguchi, T.; Niiyama, T.; Miya, K.; Taniguchi, M. *Nature Photonics* **2009**, *3* (10), 591−594.
(7) Giovannetti, G.; Khomyakov, P. A.; Brocks, G.; Kelly, P. J.; Brink, J. *Phys. Rev. B* **2007**, *76*, 073103.
(8) Ramasubramaniam, A. *Nano Lett.* **2011**, *11* (3), 1070−1075.
(9) Lee, C. G.; Li, Q.; Kalb, W.; Liu, X.; Berger, H.; Carpick, R. W.; Hone, J. *Science* **2010**, *328*, 76−80.
(10) Dean, C. R.; Young, A. F.; Meric, I.; Lee, C.; Wang, L.; Sorgenfrei, S.; Watanabe, K.; Taniguchi, T.; Kim, P.; Shepard, K. L.; Hone, J. *Nature Nanotechnol.* **2010**, *5*, 722−726.
(11) Song, L.; Ci, L.; Lu, H.; Sorokin, P. B.; Jin, C.; Ni, J.; Kvashnin, A. G.; Kvashnin, D. G.; Lou, J.; Yakobson, B. I.; Ajayan, P. M. *Nano Lett.* **2010**, *10*, 3209−3215.
(12) Shi, Y.; Hamsen, C.; Jia, X.; Kim, K. K.; Reina, A.; Hofmann, M.; Hsu, A. L.; Zhang, K.; Li, H.; Juang, Z.-Y.; Dresselhaus, M. S.; Li, L.-J.; Kong, J. *Nano Lett.* **2010**, *10*, 4134−4139.
(13) Frueh, S.; Kellett, R.; Mallery, C.; Molter, T.; Willis, W. S.; King'ondu, C.; Suib, S. L. *Inorg. Chem.* **2011**, *50*, 783−792.
(14) Li, X.; Zhu, Y.; Cai, W.; Borysiak, M.; Han, B.; Chen, D.; Piner, R. D.; Colombo, L.; Ruoff, R. S. *Nano Lett.* **2009**, *9* (12), 4359−4363.
(15) Regan, W.; Alem, N.; Alemán, B.; Geng, B.; Girit, Ç.; Maserati, L.; Wang, F.; Crommie, M.; Zettl, A. *Appl. Phys. Lett.* **2010**, *96*, 113102.
(16) Hoffman, D. M.; Doll, G. L.; Eklund, P. C. *Phys. Rev. B* **1984**, *30*, 6051.
(17) Stanishevsky, A.; Li, H.; Badzianb, A.; Badzianb, T.; Drawlb, W.; Khriachtchevc, L.; McDaniedl, E. *Thin Solid Films* **2001**, *398* −*399*, 270−274.
(18) Arutyunyan, N. R.; Obraztsova, E. D.; Silly, M.; Jaffrennou, P.; Attal-Tretout, B.; Loiseau, A.; Chuvilin, A. L. *Phys. Status Solidi B* **2006**, *243* (13), 3316−3319.
(19) Eremets, M. I.; Gauthier, M.; Polian, A.; Chervin, J. C.; Besson, J. M.; Dubitskii, G. A.; Semenova, Y. Y. *Phys. Rev. B* **1995**, *52*, 8854.
(20) Chakrabarti, D. J.; Laughlin, D. E. *Bull. Alloy Phase Diagrams* **1982**, *3* (1), 45−48.
(21) Predel, B. *Cu-N (Copper-Nitrogen)*; Madelung, O., Ed.; SpringerMaterials - The Landolt-Börnstein Database (http://www.springermaterials.com). DOI: 10.1007/10086090_1091.
(22) Luo, Z; Lu, Y.; Singer, D. W.; Berck, M. E.; Somers, L. A.; Goldsmith, B. R.; Charlie Johnson, A. T. *Chem. Mater.* **2011**, *23*, 1441−1447.
(23) Han, G. H.; Güneş, F.; Bae, J. J.; Kim, E. S.; Chae, S. J.; Shin, H.-J.; Choi, J.-Y.; Pribat, D.; Lee, Y. H. *Nano Lett.* **2011**, *11*, 4144−4148.
(24) Nemanich, R. J.; Solin, S. A.; Martin, R. M. *Phys. Rev. B* **1981**, *23*, 6348−6356.
(25) Zhang, Y.; Tan, Y.-W.; Stormer, H. L.; Kim, P. *Nature* **2005**, *438*, 201−204.